Research Article | Vol. 28, No. 26 / 21 December 2020 / Optics Express 38813
Optics EXPRESS

Long cavity photonic crystal laser in FDML operation using an akinetic reflective filter

SHARON M. BUTLER,[1,2,*] PRAVEEN K. J. SINGARAVELU,[1,2] LIAM O'FAOLAIN,[1,2,3] AND STEPHEN P. HEGARTY[1,2]

[1] *Centre for Advanced Photonics and Process Analysis, Cork Institute of Technology, Cork, Ireland*
[2] *Tyndall National Institute, Cork, Ireland*
[3] *Scottish Universities Physics Alliance (SUPA), School of Physics and Astronomy, St Andrews, UK*
[*] *sharon.butler@mycit.ie*

Abstract: A novel configuration of a Fourier domain mode locked (FDML) laser based on silicon photonics platform is presented in this work that exploits the narrowband reflection spectrum of a photonic crystal (PhC) cavity resonator. Configured as a linear Fabry-Perot laser, forward biasing of a p-n junction on the PhC cavity allowed for thermal tuning of the spectrum. The modulation frequency applied to the reflector equalled the inverse roundtrip time of the long cavity resulting in stable FDML operation over the swept wavelength range. An interferometric phase measurement measured the sweeping instantaneous frequency of the laser. The silicon photonics platform has potential for very compact implementation, and the electro-optic modulation method opens the possibility of modulation speeds far beyond those of mechanical filters.

1. Introduction

Sensing techniques in medical and environmental applications have shown a need for low-cost, and high performance swept wavelength lasers. Many swept source lasers consist of a broadband gain medium and a tunable optical bandpass filter to produce narrowband wavelength sweeps employing tuning mechanisms such as with a Fabry-Perot filter [1–3], polygon scanning mirror [4–6], or a micro-electromechanical mirror (MEMS) [7]. One limitation on sweep rate is the post filtering limit [1] where the filter is swept by more than the filter width during the cavity roundtrip period. In this situation, losses are increased in the cavity, drastically reducing output power eventually stopping laser action entirely.

One technique to overcome this limitation to some extent has been demonstrated by Johnson et al. [7] using a short cavity laser and operating in a passively mode-locked regime. The temporal pulses somewhat overlap in the backward sweep direction thereby maintaining laser action.

The post-filtering limit was most significantly overcome by the introduction of the FDML laser by Huber et al. in 2006 [8], by sweeping the filter at a period synchronous to the roundtrip time of the cavity as $f_{mod} = m/T$, where f_{mod} is the filter modulation frequency, T is the roundtrip time and m is an integer. A full sweep is optically stored in the cavity which overcomes the restriction of cavity build-up time as lasing does not need to build up from spontaneous emission. As the post-filtering limit is no longer a first-order limitation, the filter sweep speed becomes a limiting factor for the laser sweep rate. Due to the maximum sweep speed achievable of the filters which are typically employed (in the region of a few 100 kHz), a large cavity length is required to facilitate synchronisation of the roundtrip time and filter speed but the principle of FDML can be scaled to any cavity length solely depending on the maximum filter speed. Several developments of various FDML configurations to further increase the sweep speed and maximise performance for OCT applications have been reported [9–12]. FDML lasers are an attractive solution for swept source Optical Coherence Tomography (SS-OCT) applications owing to their ability to sweep large wavelength ranges at high sweep rates and high output power, features

#410525 https://doi.org/10.1364/OE.410525
Journal © 2020 Received 18 Sep 2020; revised 2 Nov 2020; accepted 4 Nov 2020; published 9 Dec 2020

Optics EXPRESS

which enhance optical imaging depth and image acquisition rates. Some reports of superimposed frequency combs over the sweeping wavelength have been demonstrated with a Fabry-Perot cavity placed within an FDML laser cavity [13–16] for applications such as improved coherence roll-off, a self-clocking method, depth ranging and frequency discrimination in a WDM network.

The emergence of Silicon Photonics in Photonic Integrated Circuits (PICs) has proven to be one of the leading technologies for high-speed optical interconnects owing to cost effective manufacture and integration with existing CMOS technologies producing low-cost, high-yield outputs. For this reason many versions of silicon based resonant modulators have been extensively researched such as microdisks [17], racetrack resonators [18,19] and microring resonators [20–22]. Electro-optical modulation of a 2D PhC cavity using a p-n junction by carrier induced refractive index change has also been demonstrated [23]. PhC cavities have a small modal area resulting in a small footprint making them an advantageous for application in PICs and integrated optical devices.

In previous work, we demonstrated a hybrid III-V/silicon PhC laser [24], using a reflective semiconductor optical amplifier (RSOA) and a vertically coupled silicon PhC cavity [25]. Frequency Modulation (FM) of the hybrid laser was achieved [26] by thermal tuning of the PhC resonance by application of voltage to a p-n junction in which the PhC cavity was embedded. In this single mode regime, the maximum continuous tuning range was limited by the laser cavity Free Spectral Range (FSR). In order to extend the continuous tuning range, a highly multimode FDML configuration was studied in this work. This configuration used the same SiN waveguide, p-n junction and silicon PhC cavity resonator as the single-mode laser and by extending the length of the laser cavity, many longitudinal modes lay within the reflectance bandwidth. Applying the principle of FDML operation, the modulation frequency matched the cavity frequency and the full spectrum was stored in the laser delay line. Using a 2 km fiber delay line within the laser cavity, the corresponding sweep frequency was applied to examine the wavelength sweep range, instantaneous frequency and temporal dynamics of this laser in FDML operation.

Reports of FDML lasers typically involve a ring cavity design with uni-directional lasing and sweeping of an optical bandpass filter [8–10]. Such lasers enforce uni-directional lasing via optical isolators, a major barrier to compact and integrated devices. For this work, a linear Fabry-Perot cavity with bi-directional lasing was implemented with forward biasing and a sine wave modulation applied to the reflector. This is the first time, to our knowledge, that a tunable PhC cavity reflector has been used to demonstrate an FDML laser.

2. Laser configuration and experimental setup

The laser cavity consisted of a broadband fiber reflector facet, a non-isolated fiber pig-tailed SOA (Kamelian OPA-20-N-C-FA, optical gain centered at 1550 nm), a polarisation controller, a fiber delay line and a lensed fiber coupled to the PhC reflector which acted as the other facet (Fig. 1(a)). The lensed fiber was actuated by a 5-axis manual translation stage.

As demonstrated by Welna et al. [27], this design of a Dispersion Adapted (DA) PhC cavity is expected to contain multiple reflection peaks, separated by the resonator FSR, each with a different bandwidth and reflectivity (Fig. 1(b)). The resonances of interest for the experiments described here i.e. 1538 nm and 1558 nm had a reflectivity of approximately 0.5 and 0.35, and reflection bandwidth of 0.6 nm and 1 nm, respectively. The PhC cavity FSR was ~7 nm which was most notable for resonances at 1591 nm, 1598 nm, and 1605 nm. The absence of visible reflection peaks at the expected wavelengths can be attributed to low reflectivity of those resonance modes and therefore are not visible on the reflection spectrum.

Below threshold, these multiple reflection peaks were also visible in the laser amplified spontaneous emission (ASE) spectrum (Fig. 1(a): inset). An increase of the gain could result in multiple resonances lasing and selection of one was possible using the polarisation controller within the laser cavity.

Optics EXPRESS

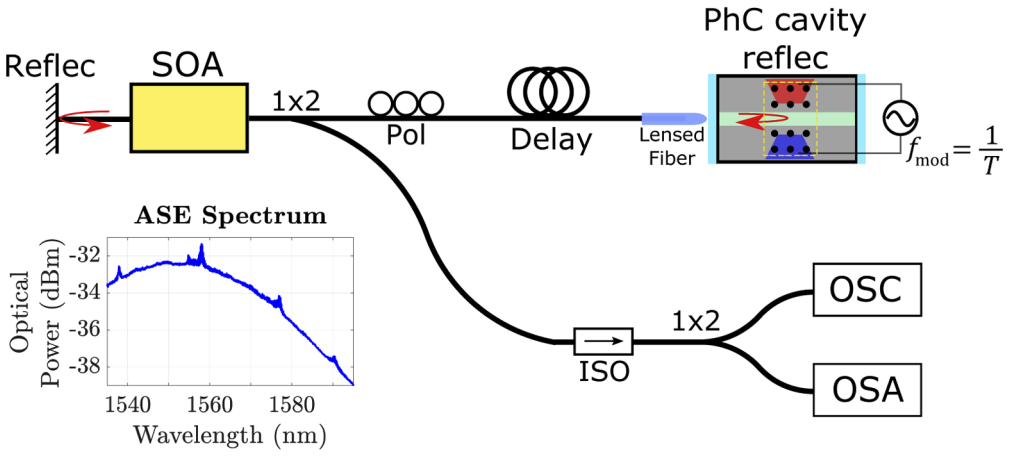

(a)

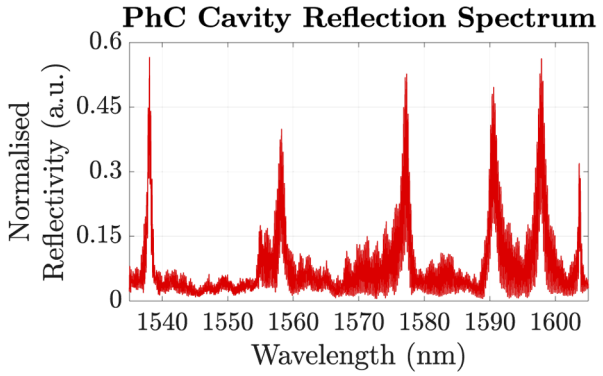

(b)

Fig. 1. (a) Laser configuration consisting of a fiber reflector, SOA, polarisation controller (Pol), fiber delay line to a lensed fiber coupled to waveguide and PhC cavity. Measurements taken from intra-cavity splitter to isolator (ISO) divided to oscilloscope (OSC) and optical spectrum analyser (OSA). Inset: Laser ASE spectrum below threshold at 30 mA. (b) Broadband ASE characterisation of PhC cavity reflection spectrum normalised to ASE source, showing multiple reflection peaks of the PhC cavity resonance modes.

Optics EXPRESS

A 50/50 1x2 splitter was included in the cavity and acted as the cavity output coupler. The light was passed through an isolator to minimise back reflections, then divided between an optical spectrum analyser and to a high-speed InGaAs photodetector connected to an oscilloscope to examine the laser intensity dynamics and optical spectrum.

3. Laser characteristics and tuning of PhC reflector

The laser showed a threshold value of 35 mA with a slope efficiency of 0.14 mW/mA and 11 mW power at maximum bias current of 120 mA (Fig. 2(a)). At pump biases just above threshold, the lasing spectrum showed a single peak. There were expected to be multiple longitudinal modes lasing within this single peak due to the small FSR (~1.2 fm) of the 2 km cavity but these were not visible due to the resolution of the OSA which was 20 pm. As the pump power was increased, the adjacent peaks began lasing and the full bandwidth of the reflector was evident from the envelope containing the narrower peaks (Fig. 2(b)). The narrower peaks stem from the multiple parasitic reflections from the PhC cavity to the chip facet superimposed on the PhC reflectance peak. Broadening of the lasing spectrum as the pump power was increased was due to more groups of longitudinal modes overcoming loss and starting to lase. There were approximately 10^6 longitudinal modes within the reflection bandwidth of ~1 nm for the 2 km cavity.

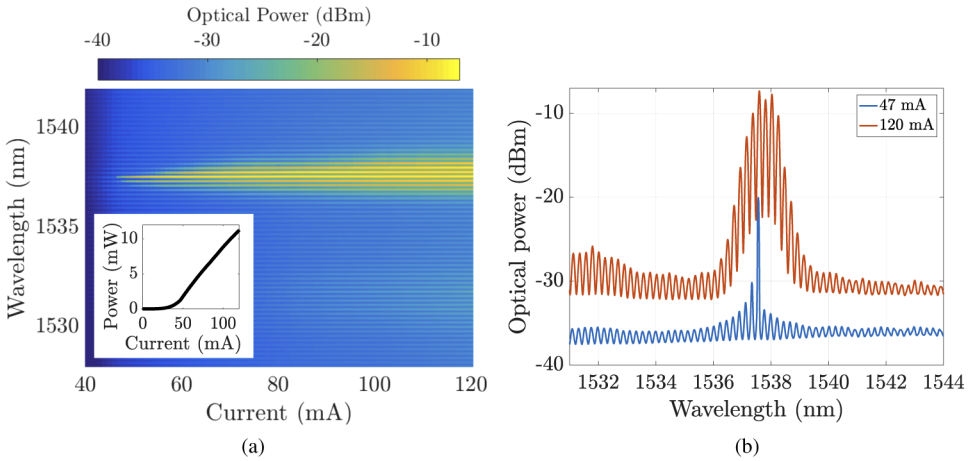

Fig. 2. Lasing characteristics of the long cavity laser. (a) Increasing SOA pump current with colourmap of OSA spectrum. Inset: LI curve. (b) OSA plots for 47 mA and 120 mA showing broadening of lasing spectrum.

As described in our previous work for single mode operation [26], a forward DC bias voltage applied to the reflector causes tuning of the PhC cavity resonance wavelength via the thermo-optic effect in silicon. DC voltage was applied to the contact pads on the p-n junction using needle probes and a DC voltage source. The SOA was biased at a fixed current of 70 mA and voltage to the p-n junction was stepped from 0-6 V in steps of 0.2 V. As a result of heating in the PhC cavity, the reflection spectrum red-shifted and the lasing spectrum consequently shifted (Fig. 3). The characteristic shape of the p-n IV curve was also apparent in the lasing spectrum shift. The p-n junction showed a "switch-on" after 1.8 V in forward bias (Fig. 3: inset) and with increasing voltage, the power dissipated non-linearly to give the quadratic curve. This gave a total wavelength red-shift of ~10 nm for this applied voltage range.

The instability of the multimode operation can be seen from the time averaged spectrum where multiple mode groups were active and lasing asynchronously. Figure 4(a) shows three captures from the OSA taken at ~10 second intervals illustrating the unstable lasing mode

Optics EXPRESS

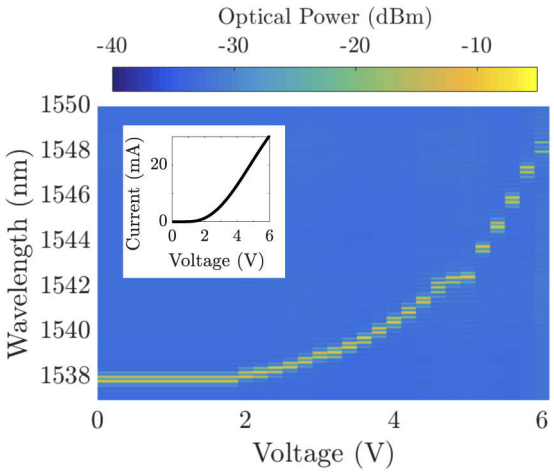

Fig. 3. Lasing spectrum shift with application of DC voltage steps to p-n junction contact pads with SOA pumping current at 70 mA. Inset: IV curve of p-n junction.

groups. The unstable lasing was also visible on the output intensity time trace showing large intensity fluctuations (Fig. 4(b)). Intensity oscillations in the GHz region were observed within the bandwidth of the 33 GHz photodetector. The instabilities observed over the seconds time range can be attributed to environmental fluctuations.

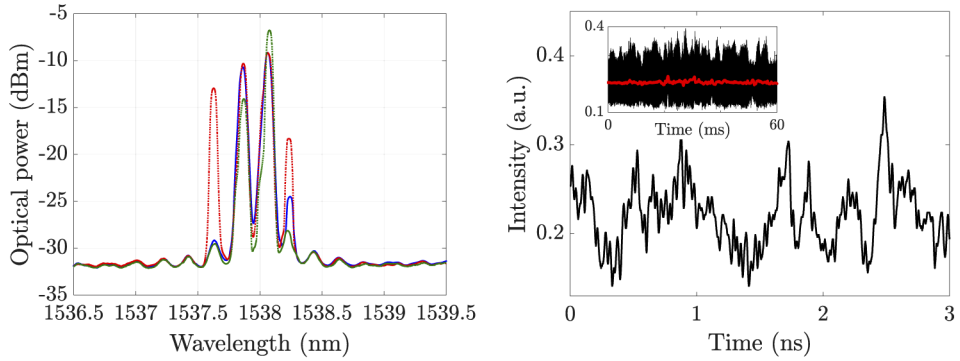

Fig. 4. (a) OSA of 3 captures of lasing spectrum at ~10 second intervals. (b) Laser intensity time trace ns scale showing large power fluctuations. Inset: ms scale intensity (black) and smoothed average intensity (red).

With fixed biases, the laser output intensity was unstable as a result of groups of multiple longitudinal modes lasing asynchronously without a fixed phase relationship. This behaviour is typical of multimode lasers due to mode competition for gain, mode switching and energy dispersion in the cavity [28]. For ring lasers with a static filter, regimes typically vary from continuous wave to chaotic depending on the spectral transmission at the filter position [29]. Multimode regimes for a short cavity swept laser have been analysed in detail in [30] showing mode-locked pulsations, mode-hopping and chaotic regimes depending on the sweep direction. Their report showed at the turning points of the sweep (where the filter moves slowest), multiple mode-hopping dynamics occurred comparable to a static filter. Detailed dynamics of an FDML

Optics EXPRESS

laser have been analysed in [31], showing the multimode instabilities present in the long cavity laser.

4. Modulation of PhC reflector

On application of a sine wave modulation of the appropriate frequency to the reflector, sweeping of the laser wavelength with a relatively stable and more predictable intensity can be obtained. A bias-tee, a DC voltage source and a function generator were combined to give a 3.9 V DC offset and 2.8-5 V sine wave modulation of the p-n junction in order to modulate the reflectance peak. The roundtrip time of the Fabry-Perot laser cavity, $T = 2nL/c$, was estimated to be 20 μs with $n_{glass} = 1.5$ and $L = 2$ km. Hence, the modulation frequency, $f_{mod} = 1/T$ was calculated as 50 kHz. This value was apparently close to the roundtrip frequency as the resulting wavelength sweep on the OSA began to stabilise and remain active in parts, mostly at the extremities of the sweep with a range of ~3.5 nm. However, the spectrum still showed some instabilities (similar to the static reflector shown in the previous section) and not active at all in other parts of the sweep (Fig. 5(a)).

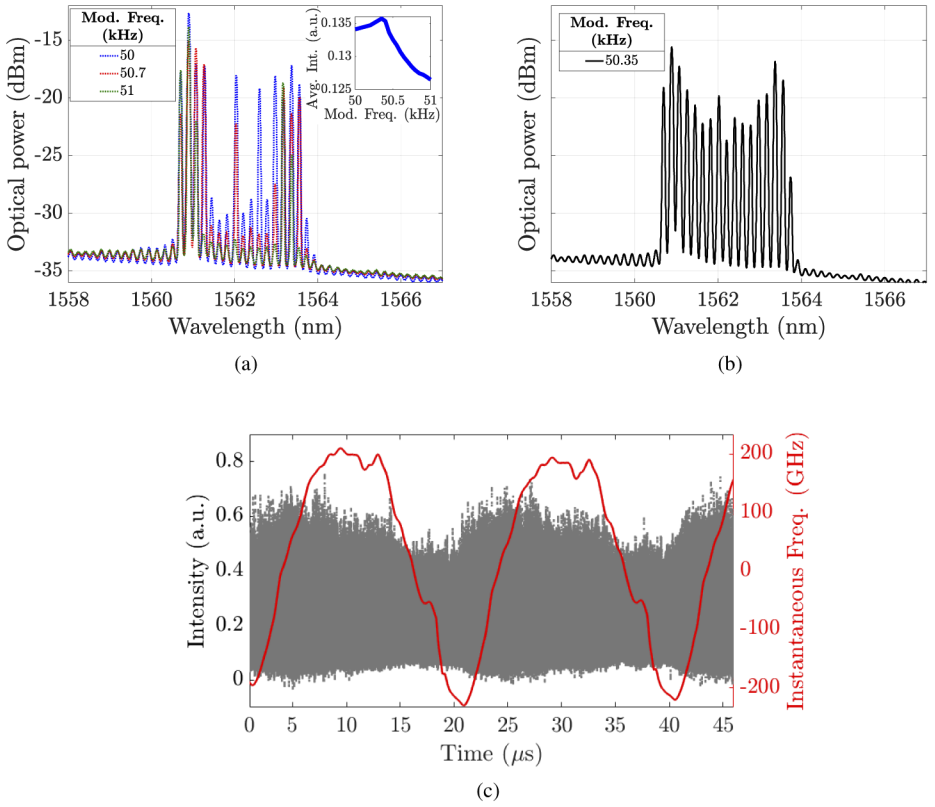

Fig. 5. OSA spectrum of swept laser (a) for modulation frequencies of 50, 50.7 and 51 kHz and average intensities as a function of modulation frequency (inset) and (b) at 50.35 kHz stable with ~3.5 nm sweep range. (c) Laser intensity (grey) with calculated instantaneous frequency from 3x3 measurement (red).

The modulation frequency was increased in steps of 0.01 kHz and the average spectral power was recorded (Fig. 5(a): inset). The power increased to a maximum and then began to decrease and the modulation frequency with the maximum power was determined to be 50.35 kHz. At this frequency, the wavelength spectrum remained stable and showed the highest power at

Optics EXPRESS

the extremities of the sweep, indicating the turning points where the reflector moves slowest (Fig. 5(b)). Deep modulation fringes (comb lines) of ~18 dB with a period of 0.18 nm were also present across the spectrum. The fringe period is closely related to the parasitic reflection peaks observed on the reflection spectrum, imposed by the reflections from the PhC cavity to the chip facet and act as an internal Fabry-Perot cavity within the larger laser cavity. By using chips with lower reflectivities, the power in these fringes can be reduced.

The swept laser intensity had a cyclic amplitude envelope repeating with each sweep period (Fig. 5(c)) with a stable average output power. Although, on a shorter time scale (ns), the intensity showed instabilities and deep modulations likely due to low coherence caused by the parasitic reflections within the cavity however, the overall intensity envelope was stable and periodic. In comparison to the static reflector case above where the intensity and average output power had large and unpredictable fluctuations, the long term stable state of the laser undergoing FDML operation was evident.

An interferometric technique for measuring the instantaneous frequency previously described by Butler et al. [32] was used to reconstruct the complex electric field of the swept laser. The instantaneous frequency is plotted as the deviation around the central frequency which is set to zero (Fig. 5(c)). The scaling factor for the instantaneous frequency is determined from the full wavelength sweep range on the OSA using the maximum and minimum wavelength values to determine the frequency range. This shows a periodic frequency sweep with a range of ~450 GHz at the synchronised modulation frequency of 50.35 kHz. The intensity envelope shows some asymmetry with the sweep direction but repeats with the same cyclic amplitude variation with the period of the sweeping instantaneous frequency.

5. Conclusion

In this work, we presented a novel configuration of an FDML laser using a tuning mechanism previously unreported exploiting the tuning capability of the narrowband PhC resonant reflector. We observed when the PhC reflector was static, multiple longitudinal mode groups were lasing unstably within the reflection band which saw unstable output. When the reflector was modulated synchronously to the delay time of the cavity, applying $f_{mod} = 1/T$, stable lasing over a sweeping wavelength range of ~3.5 nm was observed. Direct measurement of the laser phase confirmed sweeping of the laser instantaneous frequency over a range which was only limited by the maximum modulation depth achievable with the PhC cavity modulator available.

A frequency comb was generated over the swept wavelength range, atypical of traditional FDML approaches, which we attributed to the parasitic reflections from the chip facet to PhC reflector. These reflections acted as an internal Fabry-Perot cavity within the laser cavity. Although the reflections within the FDML laser presented here are considered parasitic, they can have some useful applications as demonstrated in [13–16] with the intentional placement of a Fabry-Perot cavity in an FDML laser cavity. Given that the chips used for these experiments were straight non-AR coated facets, a reduction of the comb line depth is possible for chips with lower reflectivities. We observed a reduction of the comb line depth for AR coated chips with angled waveguides to ~7 dB. However, these devices showed a lower sweep range as the modulator employed was a less efficient microheater therefore, for these experiments, we demonstrated the device with a larger sweep range with the drawback of greater parasitic reflectivities. Further improvements of the AR coating design is expected further reduce the chip facet reflectivities.

This configuration has potential as a compact on-chip solution of an FDML laser employing waveguides on-chip as the delay line of the cavity. The capability of operation in bi-directional lasing eliminates the need for isolators in the cavity. Debnath et al. [23] have demonstrated a similar p-n PhC cavity modulator with up to 0.5 GHz modulation speed operating in forward bias with a 20 pm wavelength shift. Therefore in principle, the cavity delay length could be in the region of 10s of cm to match this sweep speed. This shows that an increased sweep rate and

Optics EXPRESS

shorter cavity length is possible however, accompanied by a reduction in sweep range. Further improvements in fabrication of the PhC cavity modulators are on-going and aims to increase the modulation depth for higher modulation speeds which will lead to a wider sweep range. This would ultimately achieve a more compact solution while being capable of higher sweep speeds.

The sweep range demonstrated is considerably less than existing FDML lasers (with typical sweep ranges of ~100 nm) therefore, this laser may not yet be useful for SS-OCT applications. Given the current limitations of this laser, it can be useful in applications where a narrow sweep range is sufficient such as surface analysis [33] or microwave waveform generation [34]. Again, with improvement in fabrication of the modulator employed, the sweep range can be increased and could then find applications where moderate sweep ranges and very fast sweep speeds are required, with the added advantage of being a fully integrated device.

Funding

Science Foundation Ireland (SFI 12/RC/2276, SFI 12/RC/2276_P2 (Irish Photonic Integration Centre), SFI 16/ERCS/3838); European Research Council (Starting Grant 337508); Scottish Enterprise; Cork Institute of Technology (RISAM); Irish Government's Programme for Research in Third Level Institutions, Cycle 5, Strand 1a (CREATE); Horizon 2020 Framework Programme (Project PICCOLO (732111)).

Disclosures

The authors declare no conflicts of interest.

References

1. R. Huber, M. Wojtkowski, K. Taira, and J. G. Fujimoto, "Amplified, frequency swept lasers for frequency domain reflectometry and OCT imaging: design and scaling principles," Opt. Express **13**(9), 3513–3528 (2005).
2. M. A. Choma, K. Hsu, and J. A. Izatt, "Swept source optical coherence tomography using an all-fiber 1300-nm ring laser source," J. Biomed. Opt. **10**(4), 044009 (2005).
3. C. Jun, M. Villiger, W.-Y. Oh, and B. E. Bouma, "All-fiber wavelength swept ring laser based on Fabry-Perot filter for optical frequency domain imaging," Opt. Express **22**(21), 25805–25816 (2014).
4. E. C. W. Lee, J. F. de Boer, M. Mujat, H. Lim, and S. H. Yun, "In vivo optical frequency domain imaging of human retina and choroid," Opt. Express **14**(10), 4403–4411 (2006).
5. W.-Y. Oh, B. J. Vakoc, M. Shishkov, G. J. Tearney, and B. E. Bouma, ">400 kHz repetition rate wavelength-swept laser and application to high-speed optical frequency domain imaging," Opt. Lett. **35**(17), 2919–2921 (2010).
6. S. H. Yun, C. Boudoux, G. J. Tearney, and B. E. Bouma, "High-speed wavelength-swept semiconductor laser with a polygon-scanner-based wavelength filter," Opt. Lett. **28**(20), 1981–1983 (2003).
7. B. Johnson, W. Atia, M. Kuznetsov, B. D. Goldberg, P. Whitney, and D. C. Flanders, "Long-to-short wavelength swept source," Opt. Express **26**(26), 34909–34918 (2018).
8. R. Huber, M. Wojtkowski, and J. G. Fujimoto, "Fourier Domain Mode Locking (FDML): A new laser operating regime and applications for optical coherence tomography," Opt. Express **14**(8), 3225–3237 (2006).
9. W. Wieser, B. R. Biedermann, T. Klein, C. M. Eigenwillig, and R. Huber, "Multi-Megahertz OCT: High quality 3D imaging at 20 million A-scans and 4.5 GVoxels per second," Opt. Express **18**(14), 14685–14704 (2010).
10. T. Klein, W. Wieser, L. Reznicek, A. Neubauer, A. Kampik, and R. Huber, "Multi-MHz retinal OCT," Biomed. Opt. Express **4**(10), 1890–1908 (2013).
11. J. P. Kolb, T. Pfeiffer, M. Eibl, H. Hakert, and R. Huber, "High-resolution retinal swept source optical coherence tomography with an ultra-wideband Fourier-domain mode-locked laser at MHz A- scan rates," Opt. Express **9**(1), 120–130 (2018).
12. W. Wieser, T. Klein, W. Draxinger, and R. Huber, "Fully automated 1.5 MHz FDML laser with 100 mW output power at 1310 nm," in *Optical Coherence Imaging Techniques and Imaging in Scattering Media, SPIE Proceedings (Optical Society of America, 2015)*, vol. 9541 (2015), pp. 16–19.
13. N. Lippok, M. Siddiqui, B. J. Vakoc, and B. E. Bouma, "Extended Coherence Length and Depth Ranging Using a Fourier-Domain Mode-Locked Frequency Comb and Circular Interferometric Ranging," Phys. Rev. Appl. **11**(1), 014018 (2019).
14. M. Wan, F. Li, X. Feng, X. Wang, Y. Cao, B.-O. Guan, D. Huang, J. Yuan, and P. K. A. Wai, "Time and Fourier domain jointly mode locked frequency comb swept fiber laser," Opt. Express **25**(26), 32705–32712 (2017).
15. T.-H. Tsai, C. Zhou, D. C. Adler, and J. G. Fujimoto, "Frequency comb swept lasers," Opt. Express **17**(23), 21257–21270 (2009).

Optics EXPRESS

16. Q. Liu, Y. Wang, Z. Li, P. Shen, Y. Hou, H. Wang, and L. Liang, "High-speed interrogation system of multi-encoding weak FBGs based on FDML wavelength swept laser," Opt. Laser Technol. **107**, 54–58 (2018).
17. M. R. Watts, W. A. Zortman, D. C. Trotter, R. W. Young, and A. L. Lentine, "Vertical junction silicon microdisk modulators and switches," Opt. Express **19**(22), 21989–22003 (2011).
18. P. Dong, W. Qian, H. Liang, R. Shafiiha, D. Feng, G. Li, J. E. Cunningham, A. V. Krishnamoorthy, and M. Asghari, "Thermally tunable silicon racetrack resonators with ultralow tuning power," Opt. Express **18**(19), 20298–20304 (2010).
19. J.-B. You, M. Park, J.-W. Park, and G. Kim, "12.5 Gbps optical modulation of silicon racetrack resonator based on carrier-depletion in asymmetric p-n diode," Opt. Express **16**(22), 18340–18344 (2008).
20. F. Gardes, A. Brimont, P. Sanchis, G. Rasigade, D. Marris-Morini, L. O'Faolain, F. Dong, J. Fedeli, P. Dumon, L. Vivien, T. Krauss, G. Reed, and J. Martí, "High-speed modulation of a compact silicon ring resonator based on a reverse-biased pn diode," Opt. Express **17**(24), 21986–21991 (2009).
21. Q. Xu, S. Manipatruni, B. Schmidt, J. Shakya, and M. Lipson, "12.5 Gbit/s carrier-injection-based silicon micro-ring silicon modulators," Opt. Express **15**(2), 430–436 (2007).
22. P. Dong, W. Qian, H. Liang, R. Shafiiha, N.-N. Feng, D. Feng, X. Zheng, A. V. Krishnamoorthy, and M. Asghari, "Low power and compact reconfigurable multiplexing devices based on silicon microring resonators," Opt. Express **18**(10), 9852–9858 (2010).
23. K. Debnath, L. O'Faolain, F. Y. Gardes, A. G. Steffan, G. T. Reed, and T. F. Krauss, "Cascaded modulator architecture for WDM applications," Opt. Express **20**(25), 27420–27428 (2012).
24. A. P. Bakoz, A. A. Liles, A. A. Gonzalez-Fernandez, T. Habruseva, C. Hu, E. A. Viktorov, S. P. Hegarty, and L. O'Faolain, "Wavelength stability in a hybrid photonic crystal laser through controlled nonlinear absorptive heating in the reflector," Light: Sci. Appl. **7**(1), 39 (2018).
25. K. Debnath, K. Welna, M. Ferrera, K. Deasy, D. G. Lidzey, and L. O'Faolain, "Highly efficient optical filter based on vertically coupled photonic crystal cavity and bus waveguide," Opt. Lett. **38**(2), 154–156 (2013).
26. S. M. Butler, A. P. Bakoz, P. K. J. Singaravelu, A. A. Liles, B. O'Shaughnessy, E. A. Viktorov, L. O' Faolain, and S. P. Hegarty, "Frequency modulated hybrid photonic crystal laser by thermal tuning," Opt. Express **27**(8), 11312–11322 (2019).
27. K. Welna, S. L. Portalupi, M. Galli, L. O'Faolain, and T. F. Krauss, "Novel dispersion-adapted photonic crystal cavity with improved disorder stability," IEEE J. Quantum Electron. **48**(9), 1177–1183 (2012).
28. A. M. Yacomotti, L. Furfaro, X. Hachair, F. Pedaci, M. Giudici, J. Tredicce, J. Javaloyes, S. Balle, E. A. Viktorov, and P. Mandel, "Dynamics of multimode semiconductor lasers," Phys. Rev. A **69**(5), 053816 (2004).
29. S. Slepneva, "Dynamics of frequency swept sources for Optical Coherence Tomography," Ph.D. thesis, Cork Institute of Technology, Ireland (2015).
30. S. Slepneva, B. O'Shaughnessy, B. Kelleher, S. P. Hegarty, A. Vladimirov, H.-C. Lyu, K. Karnowski, M. Wojtkowski, and G. Huyet, "Dynamics of a short cavity swept source OCT laser," Opt. Express **22**(15), 18177 (2014).
31. S. Slepneva, B. Kelleher, B. O'Shaughnessy, S. P. Hegarty, A. Vladimirov, and G. Huyet, "Dynamics of Fourier domain mode-locked lasers," Opt. Express **21**(16), 19240–19251 (2013).
32. T. Butler, S. Slepneva, B. O. Shaughnessy, B. Kelleher, D. Goulding, S. P. Hegarty, H. C. Lyu, K. Karnowski, M. Wojtkowski, and G. Huyet, "Single shot, time-resolved measurement of the coherence properties of OCT swept source lasers," Opt. Lett. **40**(10), 2277–2280 (2015).
33. P. de Groot, "Principles of interference microscopy for the measurement of surface topography," Adv. Opt. Photonics **7**(1), 1–65 (2015).
34. J. Tang, B. Zhu, W. Zhang, M. Li, S. Pan, and J. Yao, "Hybrid Fourier-domain mode-locked laser for ultra-wideband linearly chirped microwave waveform generation," Nat. Commun. **11**(1), 3814 (2020).